Microwave spectroscopy of low-l singlet strontium Rydberg states at intermediate n, $50 \le n \le 70$

R. A. Brienza, Y. Lu, C. Wang, S. K. Kanungo, T. C. Killian, F. B. Dunning, J. J. Burgdörfer, and S. Yoshida Department of Physics and Astronomy, Rice University, Houston, Texas 77005-1892, USA
Applied Physics Graduate Program, Smalley-Curl Institute, Rice University, Houston, Texas 77005-1892, USA
Institute for Theoretical Physics, Vienna University of Technology, Vienna, Austria, EU

(Received 16 May 2023; accepted 10 August 2023; published 28 August 2023)

Microwave spectroscopy is used to measure the relative energy separations between strontium n 1S_0 , n 1P_1 , n 1D_2 , and n 1F_3 Rydberg levels for $50 \lesssim n \lesssim 70$ with uncertainties, limited by possible stray electric fields, of a few tens of kilohertz. These microwave results are used to develop a revised set of Rydberg-Ritz quantum defect parameters that can be used to predict level separations between the singlet S, P, D, and F states over a broad range of P0 with much higher precision, typically ~ 20 kHz, than is possible using earlier published parameter sets. The determination of accurate transition frequencies is central to the planning of quantum simulation experiments that involve microwave-coupled Rydberg levels, such as in the creation of Rydberg-atom synthetic dimensions.

DOI: 10.1103/PhysRevA.108.022815

I. INTRODUCTION

Atoms in highly excited states, known as Rydberg atoms, are extremely sensitive to external fields and have strong atom-atom interactions and optical nonlinearities. These properties make Rydberg atoms a popular and powerful platform for quantum computing [1,2], simulation [3–5], and optics [6]. They have great potential as sensors of DC or microwave electric fields [7] and are of interest in the study of an exotic class of molecules referred to as ultralong-range Rydberg molecules [8]. For all these applications, precise knowledge of quantum defects is needed to determine absolute term energies and level separations, and for calculating properties such as polarizabilities and the strength of Rydberg-Rydberg interactions [9]. This is especially true when employing resonant microwaves to drive Rydberg-Rydberg transitions, as is commonly used in quantum simulation experiments utilizing Rydberg atoms.

Whereas early experiments predominantly used alkalimetal atoms for Rydberg studies, recent work has demonstrated the appealing features of atomic strontium, such as access to clock transitions, isotopes lacking hyperfine structure, and the availability of bosonic singlet states that possess particularly simple level structures (see, for example, Refs. [10–15]). This level structure makes singlet states attractive when multiple coupled Rydberg levels are used in quantum simulation experiments as it reduces the possibility of unintended accidental couplings between the levels.

The use of cold gases is attractive for spectroscopic studies due to the reduced Doppler width and the opportunity to study an atom over an extended period of time. Here we focus on ⁸⁴Sr because the preparation of cold samples of this (bosonic) isotope is particularly straightforward. The transition frequencies that couple different levels are specified by their energy separation, $\Delta E_{n',l',n,l}$, which can be written as

$$\Delta E_{n',l',n,l} = -\frac{\text{Ry}_{84}}{[n' - \delta(n',l')]^2} + \frac{\text{Ry}_{84}}{[n - \delta(n,l)]^2}, \quad (1)$$

where $\mathrm{Ry}_{84} = \mathrm{Ry}_{\infty} M_{84}/(m_e + M_{84})$; Ry_{∞} is the Rydberg constant; m_e and M_{84} are the masses of the electron and the ⁸⁴Sr core ion, respectively; and $\delta(n,l)$ is the quantum defect. Quantum defects are frequently described using Rydberg-Ritz expressions of the form

$$\delta(n, l) = \delta_0(l) + \frac{\delta_2(l)}{[n - \delta_0(l)]^2} + \frac{\delta_4(l)}{[n - \delta_0(l)]^4}, \quad (2)$$

where δ_0 , δ_2 , and δ_4 are constants, and values for these parameters have been published by earlier workers for a variety of singlet strontium states [16,17]. These parameters were obtained by fitting quantum defects derived from measured term energies that, as will be discussed, were referenced to an ionization limit, E_{ion} , that differs from the current best value. For a given uncertainty, ΔE , in the measured term energy, however, the uncertainty, $\Delta \delta$, in the quantum defect increases with n as $\Delta \delta \sim n^3 \Delta E$. In consequence, quantum defects can typically only be specified to within a few digits of accuracy. Exploratory studies of the use of high-n microwavecoupled singlet states as Rydberg-state synthetic dimensions [18], however, showed that for intermediate n, $50 \lesssim n \lesssim 70$, transition frequencies predicted using these earlier Rydberg-Ritz parameters could be in error by as much as 80 MHz. For n = 60 such a difference can be reconciled by a change of only ~0.0023 in quantum defect. Indeed, in order to predict transition frequencies with a resolution of a few tens of kilohertz, quantum defects must be specified to the order of $\sim 10^{-7}$. To enable this, a detailed high-resolution spectroscopic study of the energy level separations between a variety of n ${}^{1}S_{0}$, n ${}^{1}P_{1}$, n ${}^{1}D_{2}$, and n ${}^{1}F_{3}$ states was initiated. The new microwave measurements are used to generate an updated set of Rydberg-Ritz parameters all without the need for prior knowledge of E_{ion} . The data are fit in energy space, whereupon the fitting error in each data point scales approximately with the experimental uncertainty ΔE . This is advantageous as compared to fitting the quantum defects themselves where the *n*-dependent residual $n^3 \Delta E$ biases the fitting towards highn levels with their larger uncertainties. To predict transition

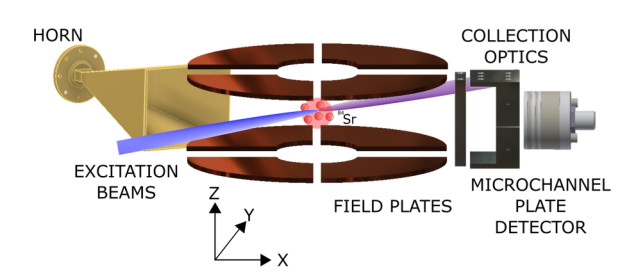


FIG. 1. Schematic diagram of the apparatus. For clarity, the laser beams used in creating the magneto-optical and optical dipole traps are not shown.

frequencies to within ~ 20 kHz for the present range of n, the Rydberg-Ritz parameters are determined to the order of 10^{-7} . Although the range of n accessible in the present work was limited by the available microwave equipment to $50 \lesssim n \lesssim 70$, the updated parameters can provide improved term separations between singlet S, P, D, and F states, and hence transition frequencies, for values of n well outside this range.

II. EXPERIMENTAL APPROACH

The present measurements were undertaken using a cold gas of 84 Sr atoms and the apparatus shown in Fig. 1. The techniques used to cool and trap strontium atoms are described in detail elsewhere [19,20]. Briefly, atoms emerging from a Zeeman slower are first cooled using a "blue" magneto-optical trap (MOT) using 461-nm light tuned to the $5s^2$ 1S_0 –5s5p 1P_1 transition. The atoms are then further cooled using a "red" MOT operating on the $5s^2$ 1S_0 –5s5p 3P_1 transition at 689 nm following which they are loaded into a 1.064- μ m crossed-sheet optical dipole trap [21]. Evaporative cooling is used to control the final atom temperature. Typically, samples of $\sim 10^5$ atoms are prepared with a peak density of $\sim 10^{11}$ cm $^{-3}$ and sample temperatures of ~ 1 –2 μ K.

Rydberg 5sns $^{1}S_{0}$ and 5snd $^{1}D_{2}$ states are created by twophoton excitation via the intermediate $5s5p^{1}P_{1}$ state using radiation at 461 and 413 nm, respectively. (The 461-nm radiation is detuned from resonance by ~19 GHz to avoid trap loss through photon scattering.) The required radiation is generated using frequency-doubled diode laser systems which also provide fundamental infrared outputs at 922 and 826 nm, respectively. These outputs are locked to an ultralowexpansion high-finesse cavity resulting in 461- and 413-nm linewidths \lesssim 15 kHz. The wavelengths of the infrared outputs were measured using a MOG Laboratories Model FZW wavemeter. This wavemeter has a resolution of $\sim \pm 30\,\mathrm{MHz}$ which, when accounting for use of two-photon excitation and frequency doubling, results in random errors in the measured optical term energies that could be as large as $\sim \pm$ 100 MHz. The wavemeter was calibrated using radiation at 844 nm which, when frequency doubled, was locked to the 422-nm $4p^6 5s {}^2S_{1/2}(F''=2)-4p^6 6p {}^2P_{1/2}(F'=3)$ transition in rubidium for which accurate measurements of the transition frequency have been reported [22]. (This calibration was checked by observing the "blow-off" of atoms from the trap as the 461-nm laser was scanned through the ${}^{1}S_{0} - {}^{1}P_{1}$ resonance. However, the corresponding transition frequency is only known to within $\pm 120 \, \text{MHz}$ [23]). The uncertainty in

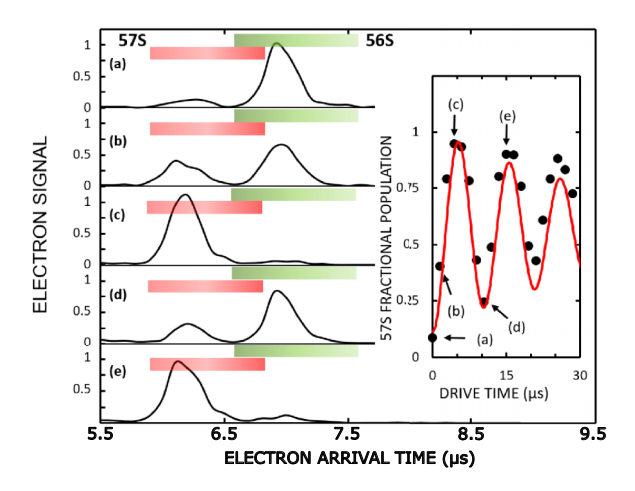


FIG. 2. Time evolution of the SFI spectrum when driving two-photon $56S \rightarrow 57S$ transitions. The shaded bars indicate the time intervals over which each state ionizes. The inset shows the measured population in the upper state as a function of the microwave drive time. The SFI spectra shown were recorded following the drive times indicated in the inset.

the wavemeter calibration is estimated to be \lesssim 30 MHz which could introduce systematic uncertainties of up to \pm 120 MHz.

The Rydberg atoms are detected by ionization in a ramped (rise time \sim 6 μ s) electric field. The product electrons are collected and directed to a dual microchannel plate for detection. Because different Rydberg states ionize at different applied fields, transitions between different nl levels can be identified through measurements of the electron arrival time distributions [24]. This is illustrated in Fig. 2, which shows the time evolution of the Rydberg population when driving two-photon $56S \rightarrow 57S$ transitions. Pronounced Rabi oscillations are seen.

Since the goal in the present work was to provide spectroscopic data for experiments involving Rydberg-atom synthetic dimensions with ten, or more, coupled Rydberg states, we focus here on Rydberg levels in the range $50 \le n \le 70$ because the microwave frequencies required to drive singleor multiphoton transitions between these levels lie in a reasonably accessible frequency regime. For example, if, as in earlier work [18], single-photon coupling of a ladder of S and Pstates is used to generate the synthetic dimension, the required frequencies range from \sim 34 GHz at n = 50 to \sim 10 GHz at n = 70. In the present studies we employ a frequency synthesizer that can be tuned from 100 MHz to 20 GHz in 1-Hz steps with an absolute accuracy of $\leq \pm 5$ kHz. Frequencies beyond this range are generated by mixing its output with that of a second radiofrequency synthesizer that can provide frequencies up to 6 GHz. The lower sidebands are not removed but play no further role in the present measurements. A K-band horn antenna is used to irradiate the atoms, which limits the range of microwave frequencies that can be covered using the present arrangement to \sim 13–26 GHz.

Initial preparation of a cold-atom sample allows for multiple subsequent measurement cycles. In each of these cycles, 20- μ s-duration laser pulses are first used to excite the Rydberg level of interest. Microwave fields are then applied. A series of approximately 1000 cycles of Rydberg excitation, microwave

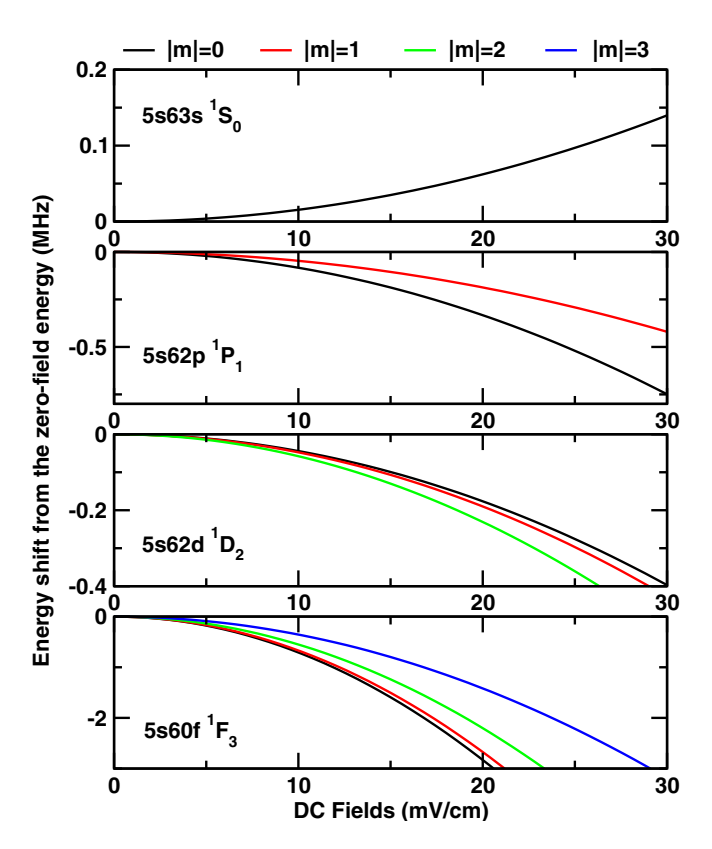


FIG. 3. Predicted Stark energy level shifts as a function of the applied DC field for the states indicated.

irradiation, and detection, each lasting about 100 μ s, can be performed using a single cold-atom sample. Typically $\lesssim 1$ Rydberg atoms are created in each laser pulse to minimize possible effects due to Rydberg-Rydberg interactions.

The energies of high-n Rydberg levels are strongly perturbed by the presence of stray electric fields. (The MOT magnetic field is turned off while taking the present data, and magnetic fields play no significant role in the present work.) To obtain energy level separations that are free of AC Stark shifts induced by the microwave fields, a Ramsey-type measurement is employed. The microwave frequency is tuned near the transition of interest. The microwave pulse duration, 0.5–1.0 μ s, is then set to generate a $\pi/2$ pulse. Next, a series of experiments is undertaken in which the atoms are initially subject to a $\pi/2$ pulse. Following some time delay during which the atoms evolve "in the dark," a second $\pi/2$ pulse is applied and the final excited-state distribution is measured as a function of this time delay. Pronounced oscillations in the populations of atoms in the upper and lower states are observed and their frequency is measured. The frequency of these Ramsey fringes corresponds to the offset between the microwave and the actual transition frequencies, thereby enabling the transition frequency to be accurately determined. To test this approach, transition frequencies were measured for a range of microwave detunings and yielded values that only varied by $\lesssim \pm 5 \, \text{kHz}$.

It is more challenging to evaluate and eliminate line shifts due to the presence of stray DC fields. Figure 3 shows DC Stark shifts representative of those that might be expected for the present range of n expressed as a function of the applied field. These (n-dependent) shifts were calculated using semiclassical dipole matrix elements for nonhydrogenic atoms [25]. The calculations suggest that, whereas for the ${}^{1}S_{0}$, ${}^{1}P_{1}$, and ${}^{1}D_{2}$ states these shifts should be small and amount to ≤ 200 kHz for stray fields of ~ 20 mV cm⁻¹, the shifts for ¹F₃ states (which lie much closer to the manifold of high-l Rydberg states) are significantly larger, ~1 MHz in a field of only $\sim 15 \text{ mV cm}^{-1}$. Stray DC fields can be canceled by application of offset fields which were determined using a procedure in which small electric fields were purposely generated in the experimental volume by applying offset potentials to the electrodes that surround it (see Fig. 1). This allows controlled electric fields to be separately applied along each of the x, y, and z axes indicated in the figure and the resulting shifts in the measured transition frequencies to be determined. These shifts were observed to vary quadratically with the applied field about some symmetry point which is taken to define the applied field necessary to null the component of the stray field along that particular axis. By iterating this technique along all three axes, we estimate that stray DC electric fields can be reduced to $\lesssim 5$ mV cm⁻¹, limiting possible DC Stark shifts for the low-l states to less than a few tens of kilohertz and to $\lesssim 200$ kHz for the ${}^{1}F_{3}$ state. Note, however, that ${}^{1}S_{0}$ levels are relatively insensitive to stray fields (see Fig. 2), and since any stray fields would induce similar Stark shifts in neighboring levels, measurement of two-photon $n^{-1}S_0$ to $n'^{-1}S_0$ transitions provide particularly accurate level separations.

III. RESULTS AND DISCUSSION

Although, as noted earlier, the systematic uncertainty associated with wavemeter calibration is relatively large, ~ 100 MHz, the present optical measurements do provide a valuable initial test of the earlier Rydberg-Ritz parameters. Table I lists the present measured term energies for a number of n $^{1}S_{0}$ and n $^{1}D_{2}$ states together with those predicted using the earlier parameters derived by Vaillant *et al.* [16] which are shown in Table II.

The observed differences between the measured and predicted energies are, typically, $\lesssim \! 100$ MHz, and their scatter is consistent with the resolution of the wavemeter.

Table I also includes quantum defects derived from the present measurements using the expression

$$\frac{\text{Ry}_{84}}{(n-\delta)^2} = E_{\text{ion}} - h\nu_1 - h\nu_2,\tag{3}$$

where the ionization energy $E_{\rm ion}$ is taken to be the updated ionization energy for ⁸⁸Sr, $\nu_{\rm ion} = E_{\rm ion}/h = 1,377,012,721$ (10) MHz recently reported by Couturier *et al.* [26] corrected for the 440(8) MHz ⁸⁸Sr - ⁸⁴Sr isotope shift [27]. $h\nu_1$ and $h\nu_2$ are the photon energies. Also included in Table I are the quantum defects predicted from earlier work [16]. Whereas the differences between the predicted and measured values, $\Delta\delta$, are small, even very small changes in quantum defect lead to significant changes in term energies and hence in energy level separations. We note that the earlier quantum defects were derived using an ionization threshold which is \sim 60 MHz lower than the most recent value [26]. This corresponds to a small but finite change in quantum defect, $\Delta\delta \sim 0.002$ for n=60.

TABLE I. Term energies and quantum defects for 5sns 1S_0 and 5snd 1D_2 states measured directly through two-photon excitation from the ground state together with those predicted using the earlier Rydberg-Ritz parameters (shown in Table II). Also included are the differences between the predicted and measured term energies, Δf , and between the predicted and measured quantum defects, $\Delta \delta$.

	Term energies			Quantum defects δ		
n	Measured (cm ⁻¹)	Predicted (cm ⁻¹)	Δf (MHz)	Predicted	Measured	$\Delta\delta$
52 <i>S</i>	45885.977	45885.97523	-53.1	3.268902	3.268107	0.000795
53 <i>S</i>	45887.813	45887.81495	58.5	3.268904	3.270144	-0.001240
55S	45891.180	45891.17949	-15.3	3.268909	3.268624	0.000285
56S	45892.723	45892.72003	-89.1	3.268910	3.266966	0.001944
57 <i>S</i>	45894.177	45894.17536	-49.2	3.268912	3.267512	0.001400
58 <i>S</i>	45895.550	45895.55165	49.5	3.268914	3.270040	-0.001130
59 <i>S</i>	45896.854	45896.85452	15.6	3.268916	3.269530	-0.000610
62 <i>S</i>	45900.373	45900.37177	-36.9	3.268920	3.267468	0.001452
63 <i>S</i>	45901.431	45901.42808	-87.6	3.268921	3.266342	0.002579
64 <i>S</i>	45902.432	45902.43265	19.5	3.268922	3.269175	-0.000250
65 <i>S</i>	45903.390	45903.38879	-36.3	3.268924	3.267199	0.001725
52D	45887.645	45887.64385	-34.5	2.364513	2.364018	0.000495
54D	45891.025	45891.02552	15.6	2.365756	2.366245	-0.000489
61 <i>D</i>	45900.257	45900.26291	177.3	2.369139	2.374258	-0.005119
64D	45903.298	45903.29403	-119.1	2.370245	2.366008	0.004237
65D	45904.207	45904.20898	59.4	2.370579	2.373087	-0.002508
66D	45905.081	45905.08116	4.8	2.370896	2.371390	-0.000494
67D	45905.910	45905.91319	95.7	2.371199	2.374708	-0.003509
68D	45906.708	45906.70750	-15	2.371489	2.370411	0.001078
69D	45907.467	45907.46634	-19.8	2.371765	2.371494	0.000271
70D	45908.191	45908.19178	23.4	2.372029	2.373494	-0.001465
71D	45908.890	45908.88575	-127.5	2.372281	2.366413	0.005868
72D	45909.550	45909.55006	1.8	2.372523	2.372402	0.000121
73 <i>D</i>	45910.185	45910.18636	40.8	2.372754	2.374395	-0.001641

Whereas a 60-MHz shift is comparable to the uncertainty in the present optical measurements, such differences can be easily resolved using microwave spectroscopy which allows transition frequencies to be determined with sub-kilohertz resolution. In consequence, microwave spectroscopy provides a particularly stringent test of Rydberg-Ritz parameters.

The measured microwave frequencies required to drive the Rydberg-Rydberg transitions indicated are shown in Table III and summarized in Fig. 4. Table III also includes transition frequencies predicted using the earlier Rydberg-Ritz parameters [16]. Sizable discrepancies of several tens of megahertz are seen between the predicted and measured values. Although these correspond to $\leqslant 0.5\%$ change in the overall transition frequency, they are, nonetheless, very important when exciting microwave-driven transitions with resolutions of a few tens of kilohertz.

The challenge is then to find values of $\delta_0(l)$, $\delta_2(l)$, and $\delta_4(l)$ for use in Eq. (2) that can predict transition frequencies with much higher precision. $\delta_2(l)$ and $\delta_4(l)$ represent the n-dependent part of the quantum defect and are governed by the term energies for low-n levels for which the interaction of the Rydberg electron with the polarized Sr^+ ion core is sizable. Therefore, we also include earlier measurements [28,29] at lower n to determine the Rydberg-Ritz parameters accurately. The optimum set of values of the Rydberg-Ritz parameters, $\delta_i(l)$ (i=0,2, and 4 and l=0,1,2, and 3) is obtained by minimizing the sum of squared residuals

$$S = \sum_{i} \left(\frac{h \nu_{n'_{i}, l'_{i}, n_{i}, l_{i}} - \Delta E_{n'_{i}, l'_{i}, n_{i}, l_{i}}}{\sigma_{i}} \right)^{2}, \tag{4}$$

where the residual between the measured transition frequency, $v_{n',l',n,l}$, and the prediction given by the Rydberg-Ritz formula,

TABLE II. Values of the Rydberg-Ritz parameters δ_0 , δ_2 , and δ_4 [see Eq. (3)] for the states of interest. The table includes both the present updated values and those reported in earlier work [16].

Earlier work			Updated			
Term	δ_0	δ_2	δ_4	δ_0	δ_2	δ_4
${}^{1}S_{0}$	3.26896	-0.138	0.9	3.2688559(1)	-0.0879(2)	-3.36(1)
${}^{1}P_{1}$	2.7295	-4.67	-157	2.7314851(1)	-5.1501(3)	-140.0(1)
$^{1}D_{2}$	2.3807	-39.41	-1090	2.3821857(14)	-40.5009(70)	-878.6(90)
${}^{1}F_{3}$	0.089	-2	30	0.0873868(8)	-1.5446(24)	7.56(1)

TABLE III. Measured transition frequencies for $nS \to nP$, $nD \to (n-3)F$, and (two-photon) $nS \to (n+1)S$ and $nS \to nD$ transitions, together with those predicted using both the earlier and the updated Rydberg-Ritz parameters listed in Table II (see text). The table also shows the corresponding differences, Δf , between the measured transition frequencies and those predicted using the earlier and updated parameter sets.

		Frequencies (MHz)		Frequency Diffe	rences Δf (MHz)
Transitions	Measured (A)	Predicted (B)	Updated (C)	(B)-(A)	(C)-(A)
56 <i>S</i> -57 <i>S</i>	43629.506	43629.677	43629.490	0.171	-0.016
57S-58S	41259.930	41260.108	41259.932	0.171	0.002
58S-59S	39058.900	39059.074	39058.909	0.174	0.002
58S-59S 59S-60S			37011.699	0.174	0.003
595-605 60 <i>S</i> -61 <i>S</i>	37011.696	37011.854 35105.243	35105.097	0.138	0.003
	35105.096				
61S-62S	33327.232	33327.373	33327.235	0.141	0.003
55S-55P	25233.565	25321.111	25233.570	87.546	0.005
56S-56P	23828.956	23911.962	23828.953	83.006	-0.003
57S-57P	22526.732	22605.510	22526.733	78.778	0.001
58S-58P	21317.747	21392.565	21317.742	74.818	-0.005
59S-59P	20193.775	20264.904	20193.780	71.129	0.005
60S-60P	19147.501	19215.160	19147.499	67.659	-0.002
61 <i>S</i> -61 <i>P</i>	18172.297	18236.713	18172.298	64.416	0.001
62S-62P	17262.228	17323.611	17262.240	61.383	0.012
63S-63P	16411.994	16470.485	16411.973	58.491	-0.021
64S-64P	15616.682	15672.490	15616.665	55.808	-0.017
65S-65P	14871.915	14925.242	14871.944	53.327	0.029
52S-52D	49961.240	50023.946	49961.261	62.706	0.021
54S-54D	44269.140	44326.267	44269.146	57.127	0.006
55S-55D	41746.116	41800.670	41746.113	54.554	-0.003
56S-56D	39411.682	39463.763	39411.637	52.081	-0.045
57S-57D	37248.428	37298.215	37248.391	49.787	-0.037
58S-58D	35240.910	35288.573	35240.930	47.663	0.020
59S-59D	33375.450	33421.029	33375.453	45.579	0.003
60S-60D	31639.562	31683.221	31639.602	43.659	0.040
61 <i>S</i> -61 <i>D</i>	30022.278	30064.055	30022.292	41.777	0.014
62S-62D	28513.498	28553.560	28513.557	40.062	0.059
63S-63D	27104.488	27142.755	27104.421	38.267	-0.067
65D-62F	19489.462	19531.258	19489.466	41.796	0.004
66D-63F	18571.873	18611.762	18571.872	39.889	-0.001
67 <i>D</i> -64 <i>F</i>	17711.111	17749.194	17711.096	38.083	-0.015
68D-65F	16902.793	16939.209	16902.801	36.416	0.008
69D-66F	16143.026	16177.854	16143.039	34.828	0.013
70 <i>D</i> -67 <i>F</i>	15428.206	15461.527	15428.216	33.321	0.010
71 <i>D</i> -68 <i>F</i>	14755.047	14786.942	14755.052	31.895	0.005
72D-69F	14120.550	14151.100	14120.552	30.55	0.003
73D-70F	13521.988	13551.253	13521.975	29.265	-0.013

 $\Delta E_{n',l',n,l_i}/h$ [Eq. (1)], is normalized by the experimental resolution σ .

The present results are for high n and, in consequence, are particularly sensitive to the value of δ_0 . However, consideration of the expansion of Eq. (2) in n^{-1} ,

$$\Delta E_{n',l',n,l} \simeq -\text{Ry}_{84} \left(-\frac{n-n'}{n^3} - \frac{\delta(n',l') - \delta(n,l)}{n^3} \right), \quad (5)$$

shows that this sensitivity is reduced for transitions between levels of the same l, i.e., l = l', since the n-independent part $\delta_0(l)$ [see Eq. (2)] cancels out when evaluating $\delta(n', l') - \delta(n, l)$. Therefore, asymptotic values of δ_0 can be more accurately extracted from transition frequencies where $l \neq l'$. The values of δ_2 and δ_4 become increasingly important as n

decreases. These parameters can be evaluated with reasonable accuracy from earlier measurements at lower n. We therefore include these earlier data in our search for optimized sets of Rydberg-Ritz parameters. The present fits were derived using our new measurements and energy level separations derived from the data selected by Vaillant $et\ al.$ in their earlier fits [28,29] (see Table IV for details). This selection avoids low-n levels where the effects of perturbing states become important and where, for D states with $n \le 15$, singlet-triplet mixing can also perturb Rydberg energy levels. To treat different data sets in an equal manner, the resolution σ is taken to be on the order of the last digit in the published transition frequency rather than the error in the measurement of δ . The Rydberg-Ritz parameters obtained through the present fits (Table II) are

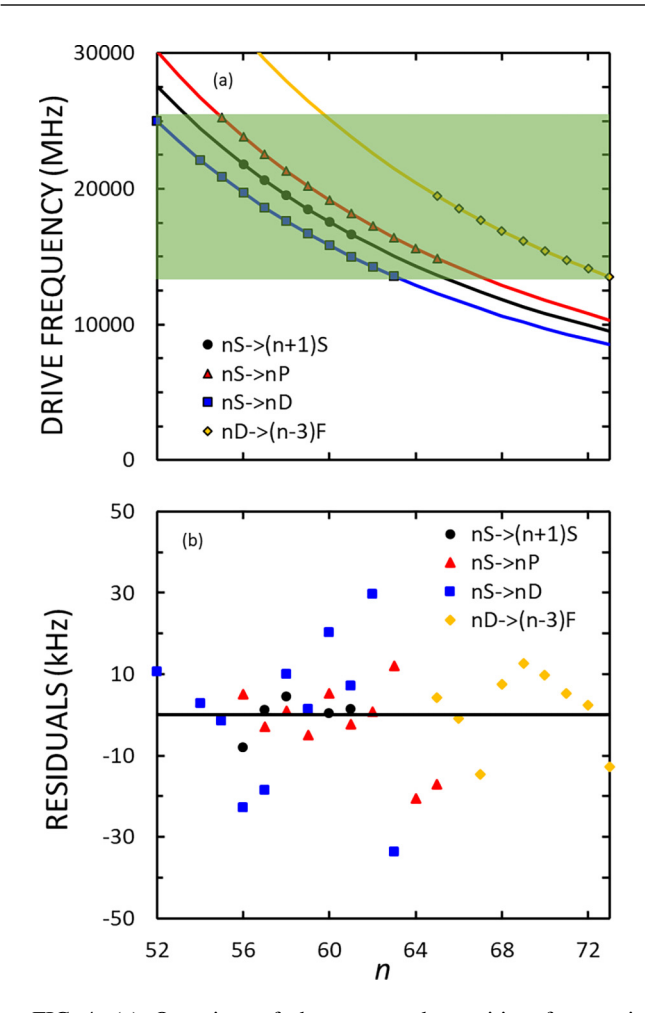


FIG. 4. (a) Overview of the measured transition frequencies (symbols) together with those predicted using the updated Rydberg-Ritz parameters (lines). For the two-photon $nS \rightarrow (n+1)S$ and $nS \rightarrow nD$ transitions the lines show one-half of the predicted term separations. For reference, the shaded region shows the range of microwave frequencies accessible using the present microwave setup. (b) Residual differences between the measured transition frequencies (symbols) and those predicted using the new updated Rydberg-Ritz parameters (see text).

TABLE IV. Data sets used for the fitting. For each transition, the N measured frequencies in the given range of n are used. The experimental resolution is set to be on the order of the last digit in the published transition frequency. For the data from Refs. [28,29] the transition frequencies between the ground state and the Rydberg states are converted to the transition frequencies between two adjacent n levels (or occasionally two next adjacent n levels when the energy of some n level is not available).

Transition	Range	σ	N	Ref.
\overline{nS} - $(n+1)S$	$56 \leqslant n \leqslant 61$	5 kHz	6	Present
nP-nS	$55 \leqslant n \leqslant 65$	5 kHz	11	Present
nD- nS	$52 \leqslant n \leqslant 63$	5 kHz	11	Present
nF- nD	$65 \leqslant n \leqslant 73$	5 kHz	9	Present
nS- $(n+1)S$	$13 \leqslant n \leqslant 32$	15 MHz	16	[28]
nD- $(n+1)D$	$20 \leqslant n \leqslant 49$	15 MHz	29	[28]
nP- $(n+1)P$	$10 \leqslant n \leqslant 28$	1.5 GHz	18	[29]
nF- $(n+1)F$	$10 \leqslant n \leqslant 24$	1.5 GHz	10	[29]

TABLE V. Transition frequencies measured earlier at high *n* [17] together with those predicted using the present updated Rydberg-Ritz parameters in Table II.

Transition	f _{meas} (MHz)	f _{pred} (MHz)	Δ_f (MHz)
$125 {}^{1}P_{1} \rightarrow 125 {}^{1}F_{3}$	9216.5	9216.8	0.3
$137 {}^{1}P_{1} \rightarrow 137 {}^{1}F_{3}$	6979.0	6979.7	0.7
$150^{-1}P_1 \rightarrow 150^{-1}F_3$	5302.5	5303.3	0.8
$160 {}^{1}P_{1} \rightarrow 160 {}^{1}F_{3}$	4361.0	4361.9	0.9
$123 {}^{1}F_{3} \rightarrow 126 {}^{1}D_{2}$	2486.8	2486.2	-0.6
$137 {}^{1}F_{3} \rightarrow 141 {}^{1}D_{2}$	4297.0	4296.2	-0.8
$148 {}^{1}F_{3} \rightarrow 152 {}^{1}D_{2}$	3412.0	3411.3	-0.7
$160 {}^{1}F_{3} \rightarrow 164 {}^{1}D_{2}$	2704.0	2702.6	-1.4

determined up to $\sim 10^{-6}$ – 10^{-7} so that transition frequencies can be evaluated up to the order of ~ 10 kHz.

As shown in Table III, use of the updated Rydberg-Ritz parameters to predict transition frequencies yields deviations from the present measured transition frequencies of typically $\lesssim 8$ kHz for 1S_0 states, $\lesssim 13$ kHz for 1P_1 states, $\lesssim 36$ kHz for 1D_2 states, and $\lesssim 9$ kHz for 1F_3 states. These residuals, $\nu_{n',l',n,l} - \Delta E_{n',l',n,l}/h$, are shown in Fig. 4 and are very much less than the values of ~ 100 kHz to 80 MHz seen when using the earlier parameters.

The Rydberg-Ritz parameters obtained using the present fitting procedure are used to generate the quantum defects shown in Fig. 5. Figure 5 also includes quantum defects obtained using the earlier Rydberg-Ritz parameters (see Table II) together with values reported in earlier studies or derived from previously published term values [28-35]. Since, as noted earlier, a given experimental uncertainty in a term value, ΔE , results in an uncertainty in the quantum defect $\Delta \delta \sim n^3 \Delta E$, the uncertainties in the quantum defects derived from measured term energies increase rapidly with n and are sensitive to the choice of ionization energy E_{ion} used in their determination. The value of E_{ion} recently reported by Couturier et al. [26] is ~60 MHz higher than the value used in analyzing much of the earlier data. (The need for such an increase was also seen in the work of Ding et al. [31,32] and an increased value was used in analysis of their data.) Reanalysis of the earlier measurements for S, P, and D states using the new value of E_{ion} results in a small increase in the values of δ which, as shown in Fig. 5, brings them into excellent agreement with the values predicted using the present Rydberg-Ritz parameters. The earlier F-state measurements of Cooke and Gallagher [30] and Fields et al. [17] were referenced to neighboring D states. Use of the updated D-state quantum defects again leads to excellent agreement with the present predictions.

Furthermore, it is reasonable to expect that the new Rydberg-Ritz parameters will enable improved calculations of energy level separations, i.e., transition frequencies, outside the present range of n. This is demonstrated by using the present Rydberg-Ritz parameters to predict level separations between a range of higher- $n^{-1}P_1$, $^{1}D_2$, and $^{1}F_3$ levels whose separations have been measured previously [17] using microwave spectroscopy. The particular transitions studied earlier are listed in Table V together with the measured energy level separations and those predicted using the present

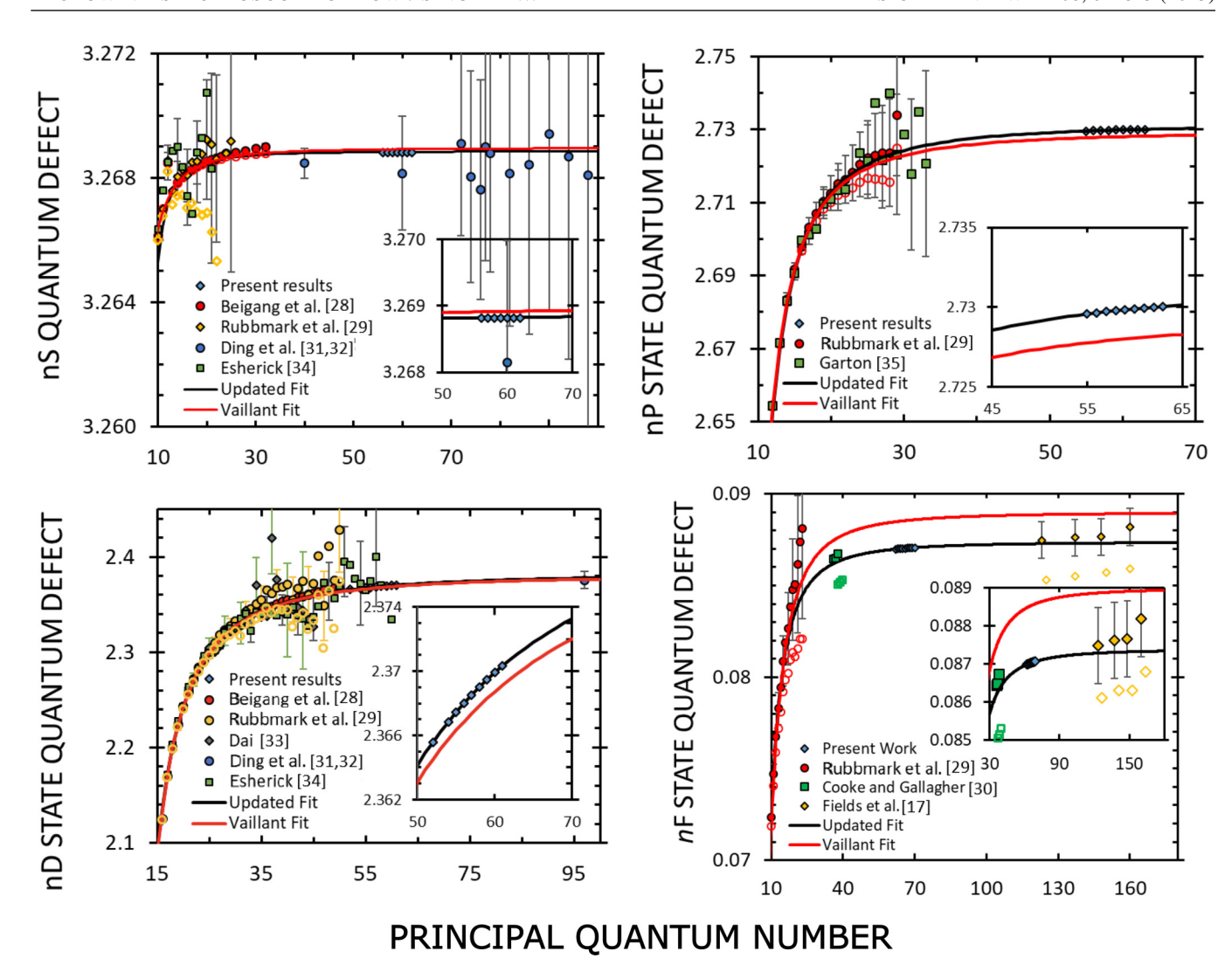


FIG. 5. Quantum defects obtained using the present updated Rydberg-Ritz parameters together with the earlier predictions of Vaillant *et al.* [16]. The figure also includes quantum defects reported in earlier studies [28,29] (open data points) and updated values (solid data points) obtained using the revised ionization energy. Also included are values derived from earlier measured term energies using the revised ionization energy. The ${}^{1}F_{3}$ values include those initially reported and those obtained after updating to the new measured ${}^{1}D_{2}$ quantum defects (see text). To better distinguish the different data sets, only representative error bars are included. The data [28,29] used in the Vaillant *et al.* fit [16] are shown in red.

Rydberg-Ritz parameters. In all cases, the agreement with experiment is very good and well within the uncertainty, ± 2 MHz, quoted in the earlier work. The new parameters therefore promise much improved estimates of level separations over a sizable range of n.

IV. CONCLUSIONS

The present work furnishes an updated self-consistent set of Rydberg-Ritz parameters that provide improved relative term energies and that can be used to accurately determine transition frequencies between different high- $n\ nl$ levels over a broad range of n. The results provide critical input when

planning quantum simulation experiments involving strontium Rydberg levels, especially those that involve many coupled levels and drive frequencies such as, for example, when Rydberg levels are used as Rydberg-atom synthetic dimensions [18], where accidental single- or multiphoton resonances could induce spurious couplings.

ACKNOWLEDGMENTS

This research was supported by the NSF under Grants No. 1904294 and No. 2110596, the FWF (Austria) under Grant No. FWF-P35539-N, and Doctoral College FWF W1243(Solids4Fun).

^[1] M. Saffman, T. G. Walker, and K. Mølmer, Rev. Mod. Phys. 82, 2313 (2010).

^[2] M. Saffman, J. Phys. B: At., Mol. Opt. Phys. 49, 202001 (2016).

^[3] S. Léséleuc, V. Lienhard, P. Scholl, D. Barredo, S. Weber, N. Lang, H. P. Büchler, T. Lahaye, and A. Browaeys, Science 365, 775 (2019).

- [4] A. Browaeys and T. Lahaye, Nat. Phys. 16, 132 (2020).
- [5] D. Barredo, H. Labuhn, S. Ravets, T. Lahaye, A. Browaeys, and C. S. Adams, Phys. Rev. Lett. 114, 113002 (2015).
- [6] O. Firstenberg, C. S. Adams, and S. Hofferberth, J. Phys. B: At., Mol. Opt. Phys. 49, 152003 (2016).
- [7] D. H. Meyer, Z. A. Castillo, K. C. Cox, and P. D. Kunz, J. Phys. B: At., Mol. Opt. Phys. 53, 034001 (2020).
- [8] J. P. Shaffer, S. T. Rittenhouse, and H. R. Sadeghpour, Nat. Commun. 9, 1965 (2018).
- [9] N. Šibalić, J. Pritchard, C. Adams, and K. Weatherill, Comput. Phys. Commun. 220, 319 (2017).
- [10] M. A. Norcia, M. N. Winchester, J. R. K. Cline, and J. K. Thompson, Sci. Adv. 2, e1601231 (2016).
- [11] N. Schine, A. W. Young, W. Eckner, M. J. Martin, and A. M. Kaufman, Nat. Phys. 18, 1067 (2022).
- [12] C. Lisdat, S. Dörscher, I. Nosske, and U. Sterr, Phys. Rev. Res. 3, L042036 (2021).
- [13] S. Stellmer, M. K. Tey, B. Huang, R. Grimm, and F. Schreck, Phys. Rev. Lett. 103, 200401 (2009).
- [14] J. D. Whalen, S. K. Kanungo, R. Ding, M. Wagner, R. Schmidt, H. R. Sadeghpour, S. Yoshida, J. Burgdörfer, F. B. Dunning, and T. C. Killian, Phys. Rev. A 100, 011402(R) (2019).
- [15] F. B. Dunning, T. C. Killian, S. Yoshida, and J. Burgdörfer, J. Phys. B: At., Mol. Opt. Phys. 49, 112003 (2016).
- [16] C. L. Vaillant, M. P. A. Jones, and R. M. Potvliege, J. Phys. B: At., Mol. Opt. Phys. 45, 135004 (2012).
- [17] G. Fields, R. Brienza, F. B. Dunning, S. Yoshida, and J. Burgdörfer, Phys. Rev. A 104, 032817 (2021).
- [18] S. K. Kanungo, J. D. Whalen, Y. Lu, M. Yuan, S. Dasgupta, F. B. Dunning, K. R. A. Hazzard, and T. C. Killian, Nat. Commun. 13, 972 (2022).
- [19] S. Stellmer, R. Grimm, and F. Schreck, Phys. Rev. A 87, 013611 (2013).

- [20] Y. N. Martinez de Escobar, P. G. Mickelson, M. Yan, B. J. DeSalvo, S. B. Nagel, and T. C. Killian, Phys. Rev. Lett. 103, 200402 (2009).
- [21] K. M. O'Hara, M. E. Gehm, S. R. Granade, and J. E. Thomas, Phys. Rev. A 64, 051403(R) (2001).
- [22] A. Sinclair, M. Wilson, and P. Gill, Opt. Commun. 190, 193 (2001).
- [23] J. Sansonetti and G. Nave, J. Phys. Chem. Ref. Data 39, 033103 (2010).
- [24] T. H. Jeys, G. W. Foltz, K. A. Smith, E. J. Beiting, F. G. Kellert, F. B. Dunning, and R. F. Stebbings, Phys. Rev. Lett. 44, 390 (1980).
- [25] N. B. Delone, S. P. Goreslavsky, and V. P. Krainov, J. Phys. B: At., Mol. Opt. Phys. 27, 4403 (1994).
- [26] L. Couturier, I. Nosske, F. Hu, C. Tan, C. Qiao, Y. H. Jiang, P. Chen, and M. Weidemüller, Phys. Rev. A 99, 022503 (2019).
- [27] S. Ye, X. Zhang, T. C. Killian, F. B. Dunning, M. Hiller, S. Yoshida, S. Nagele, and J. Burgdörfer, Phys. Rev. A 88, 043430 (2013).
- [28] R. Beigang, K. Lücke, A. Timmermann, P. West, and D. Frölich, Opt. Commun. 42, 19 (1982).
- [29] J. R. Rubbmark and S. A. Borgström, Phys. Scr. 18, 196 (1978).
- [30] W. E. Cooke and T. F. Gallagher, Opt. Lett. 4, 173 (1979).
- [31] R. Ding, J. D. Whalen, S. K. Kanungo, T. C. Killian, F. B. Dunning, S. Yoshida, and J. Burgdörfer, Phys. Rev. A 98, 042505 (2018).
- [32] R. Ding, Spectroscopy of ⁸⁷Sr Rydberg atoms and molecules, Ph.D. thesis, Rice University, 2019.
- [33] C. J. Dai, Phys. Rev. A 52, 4416 (1995).
- [34] P. Esherick, Phys. Rev. A 15, 1920 (1977).
- [35] W. Garton and K. Codling, J. Phys. B: At. Mol. Phys. 1, 106 (1968).